INVESTIGATING THE HOT WORKING WINDOW OF 2205 DSS USING DYNAMIC MATERIAL MODEL

[1]Elvis GONYA, [2]Charles SIYASIYA, [1]Elizabeth MAKHATHA

[1]*University of Johannesburg, Johannesburg, South Africa, elvisg@uj.ac.za, emakhatha@uj.ac.za*
[2]*University of Pretoria, Pretoria, South Africa, charles.siyasiya@up.ac.za*

Abstract

In this work, the dynamic material modelling (DMM) is employed to identify the hot working window that is suitable for hot processing of Duplex stainless steel 2205 (DSS). The Gleeble 1500 thermo-mechanical simulator was used to conduct the investigation, where several hot compression tests were conducted at a temperature range of 850 - 1050 °C and strain rates of $0.001s^{-1}$ - $5s^{-1}$. The obtained experimental data were first corrected for friction and adiabatic heating, the correction of adiabatic heating was only done for a strain rate of 1 and $5s^{-1}$. After the corrections, the corrected flow stress curves were plotted, and the flow stress data at the strain of 0.1, 0.3, 0.5 and 0,8 were generated. Using the generated flow stress data at a particular strain and combination of temperature and strain rates, the strain rate sensitivity values were calculated using constitutive modelling. The DMM was then applied to calculate the efficiencies and instability values followed by using cubic spline interpolation for more detailed data. The processing maps were then constructed from the results of cubic spline interpolation. The processing maps indicated that, the hot working process of 2205 DSS is more efficient at low strain rates and high temperatures, particularly at true strains below 0.3. With increase in strain to 0.5 and above, high efficiency seemed to spread to the regions of high strain rates and moderate high temperatures.

Keywords: Poor hot workability, dynamic material modelling, processing maps, hot working window

1.   INTRODUCTION

The 2205 DSS falls under the umbrella of stainless steels and with a unique metallurgical microstructure that contains approximately an equal proportion of austenite and ferrite phase. It tends to exhibit superior mechanical and physical properties other than the single phase austenitic and ferritic stainless steels [1]. The superior mechanical properties have earned this particular alloy several engineering applications including: marine, sugar-mills, petroleum, oil and gas industries, construction, and paper mills [1], [2]. Despite its attractiveness in various engineering industry, poor hot workability associated with this alloy pose a great challenge during hot processing. For instance, evidence of edge cracks and other structural inhomogeneities in a final rolled products are some of the manifestations of poor hot workability [3], [4].

Even though several studies have been conducted to address the issue of hot workability in 2205 DSS and other dual phase alloys under the family of stainless steel, poor hot workability remains a challenge. Solving the poor hot workability issue requires identification of hot working range where the alloy can be hot processed without suffering from structural inhomogeneities. A viable tool to identify this range is the processing map (PM) which helps to differentiate good and bad zones within the hot process. This paper is aimed at using the processing maps to identify a hot working window that is suitable for hot processing of 2205 DSS.

The PM uses a combination of two contour maps (instability and power dissipation efficiency) to separate the unsafe and safe working zones [5]. To construct the maps the power dissipation efficiency and instability values are calculated according to the approach of Marty and Rao given below:

$$\eta = 2\left(1 - \frac{1}{\sigma\dot{\varepsilon}}\left[\left(\frac{\sigma\dot{\varepsilon}}{m+1}\right)_{\dot{\varepsilon}=0.001} + \int_{0.001}^{\dot{\varepsilon}} d\dot{\varepsilon}\right]\right) \tag{1}$$

Where: η = power dissipation efficiency σ = flow stress (MPa), $\dot{\varepsilon}$ = strain rate (s^{-1}), and m = strain rate sensitivity. The instability values are calculated as follows:

$$\xi_{Murty} = 2m - \eta, \text{ and if } 2m - \eta < 0 = \text{instability} \tag{2}$$

The η, the ξ values are plotted on a logarithmic strain rate vs temperature scale to generate power dissipation efficiency and instability maps. The latter map is then overlayed on top of the former to generate a processing map. In a PM, the domains and regimes associated with stable and unstable flow respectively are clearly defined.

2.   MATERIAL AND EXPERIMENTAL PROCEDURE

The stainless-steel alloy used during this research was a 2205 DSS supplied by MULTI Alloys in the as-rolled condition and in the form of a 10mm Ø rod. To validate the as-received material, chemical analysis and microstructural analysis were conducted, and the results are shown below in **Table 1** and **Figures 1, 2.** The as-received microstructure shows austenite islands (γ-light phase) distributed uniformly within the ferrite matrix (α-brown phase) along the rolling direction. In addition, the initial volume fraction was measured using Imaje J and found to be 51% ferrite and 49% austenite.

Table 1 Chemical analysis of 2205 DSS

%C	%Si	%Mn	%P	%S	%Cr	%Ni	%Mo	%N	%Fe
0.023	0.34	1.67	0.029	0.003	22.80	5.20	3.20	0.1703	66.57
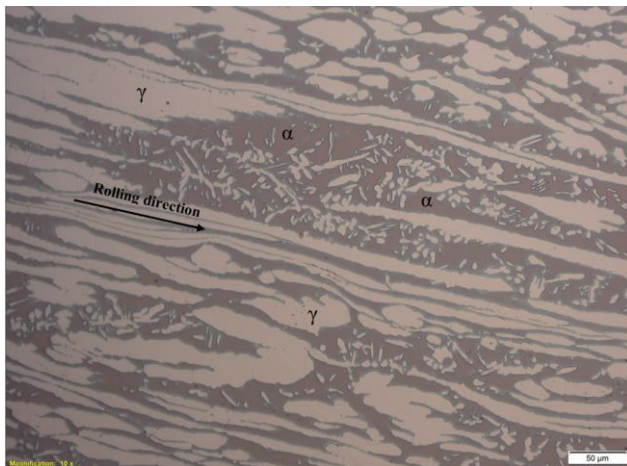
**Figure 1** Microstructure of 2205 DSS as received and as rolled
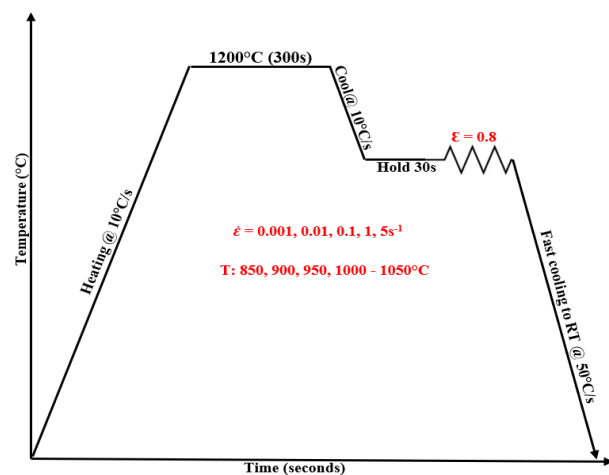
Figure 2 Hot deformation cycle of 2205 DSS

The rod was sectioned into 25 pieces of 15mm using wire cutting machine for preparation of hot compression tests in Gleeble 1500-control system programed as in **Figure 2**. All samples were then hot compressed to a total true strain of 0.8, at a temperature range of 850°C to 1050 °C with an interval of 50 °C and strain rates of 0.001, 0.01, 0.1, 1, and 5 s^1. After deformation, the deformed samples of interest were sectioned parallel to the compression axis, mount, ground and polished to 1µm diamond paste. To reveal the microstructure, polished samples were etched using 10% oxalic solution followed by examination under optical microscope.

3. RESULTS AND DISCUSSION

3.1 Single-hit flow curves

The flow curves obtained during single hit compression tests in **Figure 3** below shows that flow stress is sensitive to both temperature and strain rate. The increase in strain rate and decrease in temperature brought a decrease in flow stress. This is due to high strain rates increasing the formation of dislocation entanglements; whereas a drop in temperature lowers the kinetics of diffusional atoms. Both conditions are complicating mobile dislocations to slip during deformation, thus, necessitating the increase in applied stress. Evidence of DRX was observed at low strain rates ($<0.1s^{-1}$) and high deformation temperature (1050 °C) due to condusive deformation conditions where dislocations have enough time to build up energy for DRX due to low strain rates. High temperatures increase the kinetics of grain boundary migration and promotes faster nucleation and growth rate of DRX grains. High strain rates except those of ($15s^{-1}$) and low temperature conditions seemed to have promoted slugging DRX kinetics since a broad peak followed by the insignificant drop in flow stress was observed. At $5s^{-1}$, discontinuous yielding was observed towards the end of work hardening which could be associated with generation of new dislocations from the grain boundary or unlocking of pinned dislocations from the solutes.
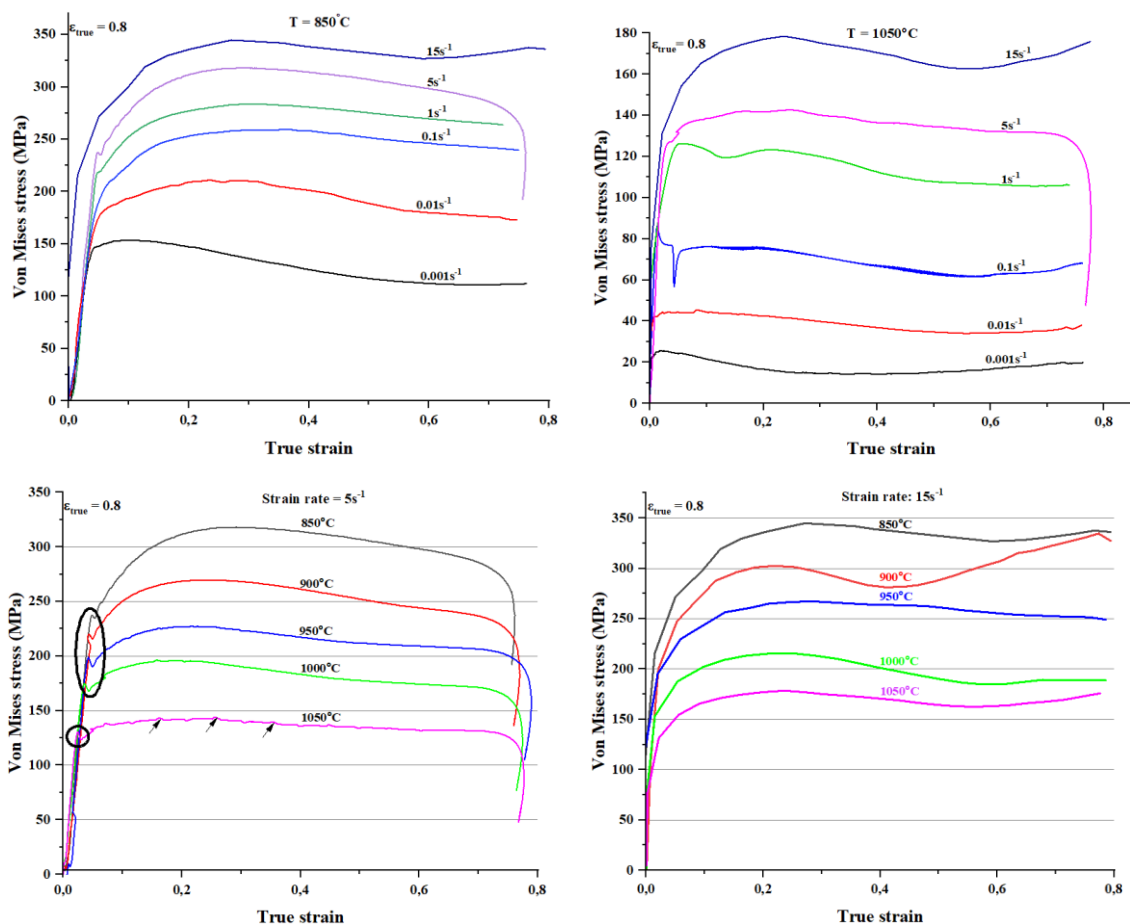

Figure 3 Single-hit flow curves at various deformation conditions

3.2 Processing maps

Construction of processing was carried out using corrected hot flow curves and Origin software 2022 version. The main reason of drawing these maps was to identify the hot working range, where 2205 DSS can be hot 9processed without suffering from microstructural inhomogeneities. As shown in **Figure 4,** the processing

maps of 2205 DSS constructed at various true strains of 0.1, 0.3, 0.5 and 0.8. The shaded (in several colours) and unshaded (contour lines) areas in a PM represented unsafe and safe hot working zones respectively. Unshaded areas marked (A, B, C) were associated with high η-values and identified conducive for hot processing of the 2205DSS whereas shaded areas are to be avoided due to risk of flow instabilities.
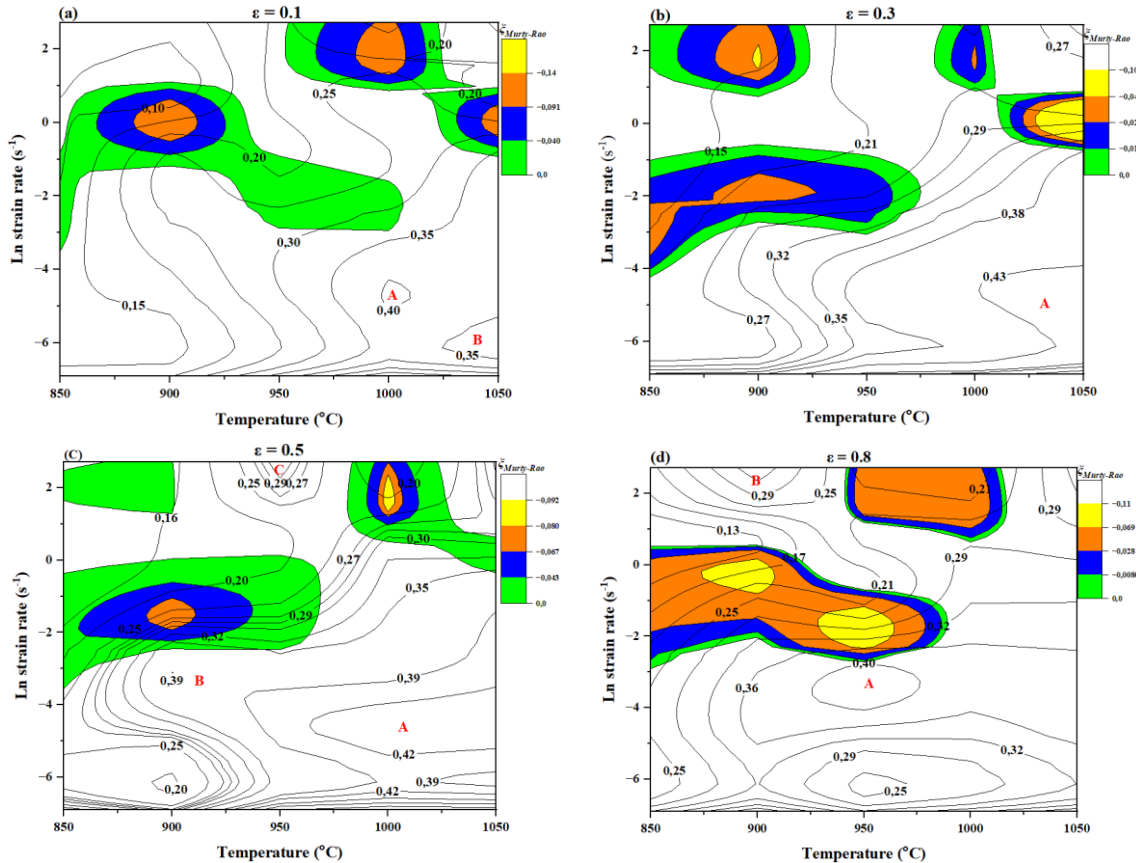
Figure 4 Processing maps of 2205 DSS constructed at various true strains of 0.1, 0.3, 0.5 and 0.8

Table 2 below summarises the ideal hot working window of 2205 DSS based on three strain rates ranges. It can be seen that low strain rates domain offers a wide temperature window which is coupled with high efficiencies across all true strains. Thus, any hot processing done at this region will result in good hot workability, refined microstructure, and improved mechanical properties. With increase in strain rates region, a narrow working window coupled with moderate efficiency was observed.

Table 2 Ideal hot working window of 2205 DSS at various range of deformation conditions

Strain rate region (s^{-1})	True strain range	Temperature range (°C)	η -range (%)
Low: 0.001 - 0.04	0.1 - 0.8	900 - 1050	29 - 43
Intermediate: 0.05 - 0.5	0.3 - 0.8	990 -1050	26 - 38
High: 10 - 15	0.7-0.8	875 - 920	24 -33

Figure 5 below shows the variation of power dissipation efficiency as a function of true strain at two extreme temperatures (850 °C and 1050 °C). It was observed that DRV was more prominent at low temperatures and relatively high strain rates (above 0,01s^{-1}). This observation was in line with what was observed from the flow curve of 850 °C presented earlier. With temperature increase to 1050 °C, lower strain rates have entered the DRX region; however, the behavior of high strain rates was similar for both temperatures.
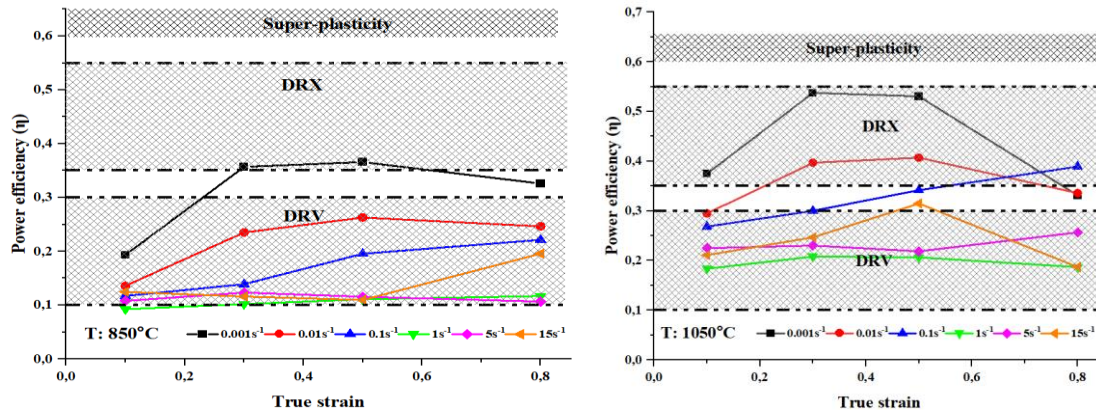
Figure 5 Variation of power efficiency as a function of strain at various deformation conditions

3.3   Microstructural analysis

The validity of processing maps was evaluated by conducting metallographic analysis of two samples that were deformed under safe and unsafe hot working conditions. The deformation conditions for each sample were: **A1**: $\varepsilon = 0.3, \dot{\varepsilon} = 8.75s^{-1}, T = 900°C$ and **A2**: $\varepsilon = 0.3, \dot{\varepsilon} = 0.0017s^{-1}, T = 1040 °C$
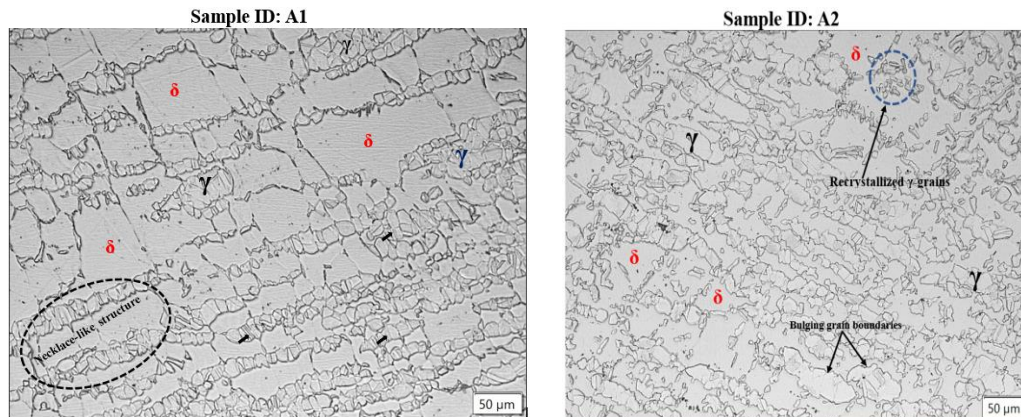
Figure 6 Optical micrographs of samples deformed at ε = 0.3

Figure 6 shows Sample A1 deformed in the unsafe region and exhibited necklace structure of austenite grains at the pre-existing ferrite boundaries. However, very few austenite grains were observed at the boundaries suggesting recrystallisation process was incomplete. Moreover, a necklace structure was compressed between the coarse ferrite grains indicating deformation was more concentrated on the austenitic phase. Since the austenitic phase is assumed to be harder than ferritic phase, non-uniform distribution of stresses is likely to have occurred between the phases, causing the formation of deformation bands on the austenite grains. The bands are indicated by black arrows on the optical micrograph. Sample A2 was deformed in a safe zone and exhibited distribution of recrystallised austenite grains along the hot working direction. The ferritic matrix was largely covered with austenite grains, suggesting the completion of DRX process. Other characteristics of recrystallisation were bulging of grain boundaries and recrystallised austenite grains as indicated in the optical micrograph.

3.4   Relevance of processing map in industrial hot forming operations

Even though low strain rates region was coupled with high efficiencies, such strain rates are not ideal for hot rolling at the rolling mill. Usually, the rolling mill encompasses the strain rates ranging from 10s^{-1} to 30s^{-1}. Therefore, it is ideal to conduct hot processing of 2205 DSS at high strain rates and low temperature regions.

4. CONCLUSION

The processing maps constructed from the results of cubic spline interpolation indicated that, the hot working process of 2205 DSS is more efficient at low strain rates and high temperatures, particularly at true strains below 0.3. With increase in strain to 0.5 and above, high efficiency seemed to spread to the regions of high strain rates and moderate high temperatures. Microstructural analysis as a tool validate the reliability of PM and confirmed the restoration mechanisms.

REFERENCES

[1] G. FARGAS, N. AKDUT, M. ANGLADA, and A. MATEO. Microstructural evolution during industrial rolling of a duplex stainless steel. *ISIJ Int.* 2008, vol. 48, no. 11, pp. 1596-1602. Available from: https://doi.org/10.2355/isijinternational.48.1596.

[2] M. ROSSO, I. PETER, and D. SUANI. About heat treatment and properties of Duplex Stainless Steels. *J. Achiev. Mater. Manuf. Eng.* 2013, vol. 59, no. 1, pp. 26-36.

[3] N. HAGHDADI, P. CIZEK, H. BELADI, and P. D. HODGSON. Dynamic Restoration Processes in a 23Cr-6Ni-3Mo Duplex Stainless Steel: Effect of Austenite Morphology and Interface Characteristics. *Metall. Mater. Trans. A Phys. Metall. Mater. Sci.* 2017, vol. 48, no. 10, pp. 4803-4820. Available from: https://doi.org/10.1007/s11661-017-4227-2.

[4] Y. ZHAO, X. LI, W. ZHANG, R. D. K. MISRA, and Z. LIU. Strain Partitioning and Softening Mechanisms of δ/γ in Lean Duplex Stainless Steels during Hot Deformation. *Steel Res. Int.* 2020, vol. 91, no. 1, pp. 1-12. Available from: https://doi.org/10.1002/srin.201900212.

[5] Y. V. R. K. PRASAD, K. P. RAO, and S. SASIDHARA. *Hot Working Guide.* 2015. [Online]. Available from: http://linkinghub.elsevier.com/retrieve/pii/B978008033454750019X